Electronic Supplementary Material (ESI) for RSC Advances.

Supplementary Information

Experimental and Theoretical Studies of DMH as Complexing Agent for Cyanide-free Gold Electroplating Electrolyte

Xuefeng Ren, Ying Song, Anmin Liu, Jie Zhang, Peixia Yang, Jinqiu Zhang, and Maozhong An*

State Key Laboratory of Urban Water Resource and Environment, School of Chemical Engineering and Technology, Harbin Institute of Technology, Harbin, 150001, China.

** Correspondence to:*

mzan@hit.edu.cn (Maozhong An), Tel/Fax: +86-451-86418616

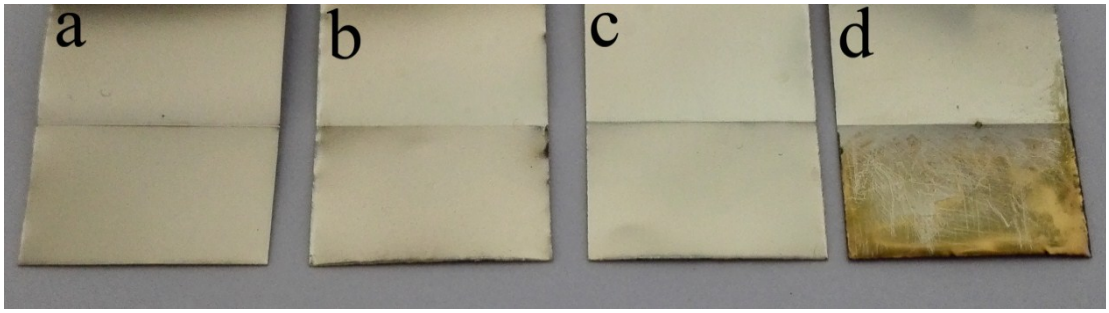

Fig. S1 Replacement reaction, (a) original surface of a copper substrate with nickel electrodeposit coated, immersed the copper substrate with nickel electrodeposit coated into the introduced cyanide-free gold electroplating electrolyte, (b) with additive, (c) without additive, and (d) the copper substrate with nickel electrodeposit coated immersed into the $HAuCl_4$ electrolyte without DMH.

As displayed in Fig. S1, after immersed the copper substrate with nickel electrodeposit coated into the introduced cyanide-free gold electroplating electrolyte with additive and without additive, no difference was observed on the surface after the immersion. Thus, as DMH employed as complexing agent in the electrolyte to coordinate with $HAuCl_4$ to form $[Au(DMH)_4]^-$, the stability of $HAuCl_4$ was significantly improved and no strike-plating process was necessary to obtain good adherent gold deposits on the substrate using the introduced gold plating electrolyte containing DMH as complexing agent. However, when the copper substrate with nickel electrodeposit coated was immersed into the $HAuCl_4$ electrolyte without DMH. Obvious replacement reaction occurred on the surface and the gold deposited on the substrate with chemical reduction by nickel, and the nickel electrodeposit dissolved into the $HAuCl_4$ electrolyte without DMH. Poorly adhering gold deposits on substrates usually result from a displacement reaction occurring between substrates and Au-complexes inside the electrolyte before electroplating. So the application of DMH as complexing agent in the electrolyte to coordinate with $HAuCl_4$ to form $[Au(DMH)_4]^-$ is very important.

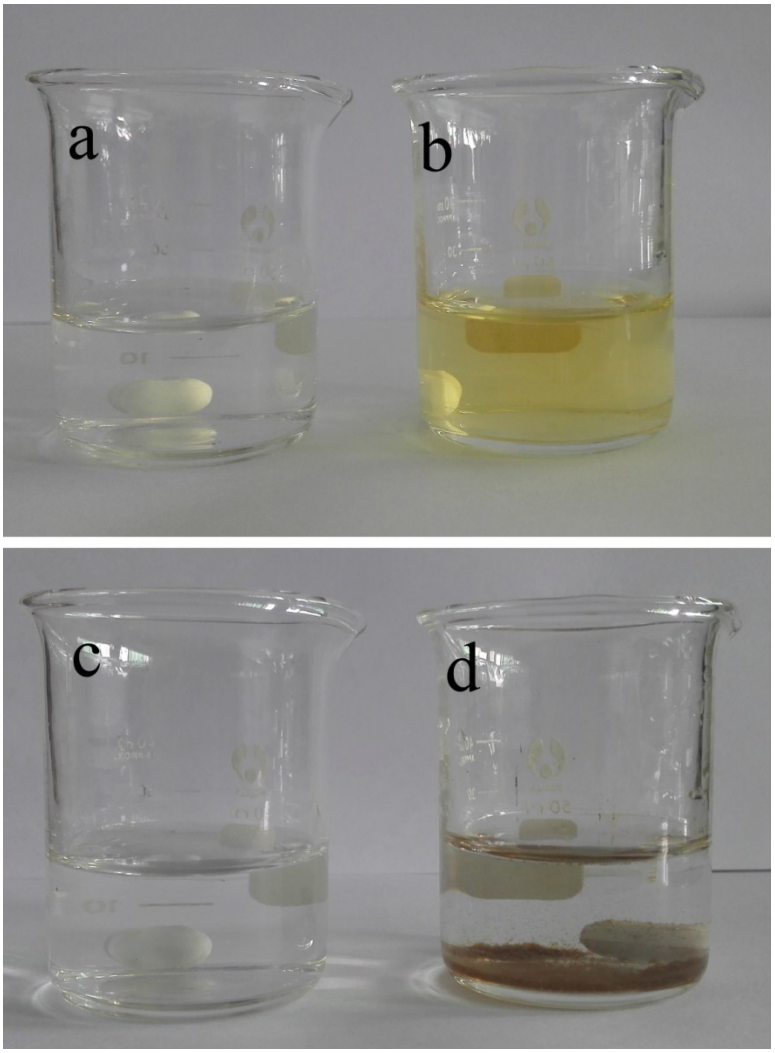

Fig. S2 Gold electroplating electrolyte used in this research, (a) new prepared gold electroplating electrolyte with additive, (b) new prepared $HAuCl_4$ electrolyte without DMH and additive, (c) gold electroplating electrolyte used for many times gold electroplating, (d) after addition of the additive into new prepared $HAuCl_4$ electrolyte without DMH.

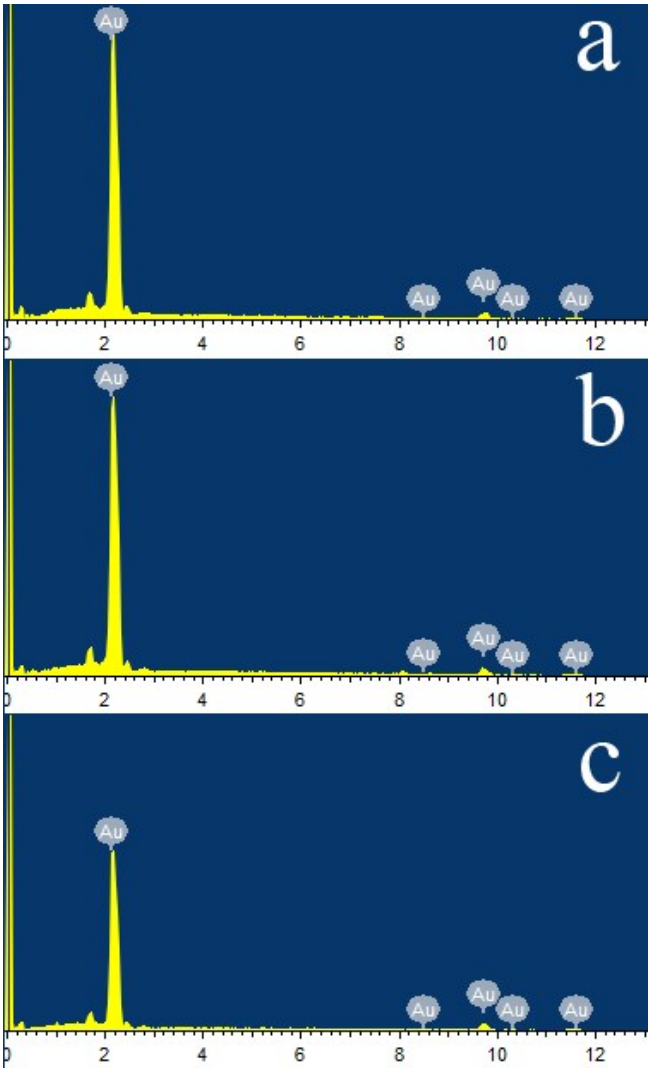

Fig. S3 The EDS patterns of gold electrodeposits obtained from the introduced cyanide-free gold electroplating electrolyte, (a) with additive, (b) without additive, and (c) from $HAuCl_4$ electrolyte without DMH.

The molecular structures of hydantoin and its usual derivatives molecules, including aminohydantoin (AHD), 1-bromo-3-chloro-5,5-dimethylhydantoin (BCDMH), 1,3-dibromo-5,5-dimethylhydantoin (DBDMH), 1,3-dichloro-5,5-dimethylhydantoin (DCDMH), dimethyloldimethyl hydantoin (DMDMH), 5,5-dimethylhydantoin (DMH), and 1,5,5-trimethylhydantoin (TMH), are shown in Fig. S4. It is of important significance to get an insight view of the reasons for selecting DMH from hydantoin derivatives as the complexing agent for the introduced cyanide-free gold electroplating electrolyte.

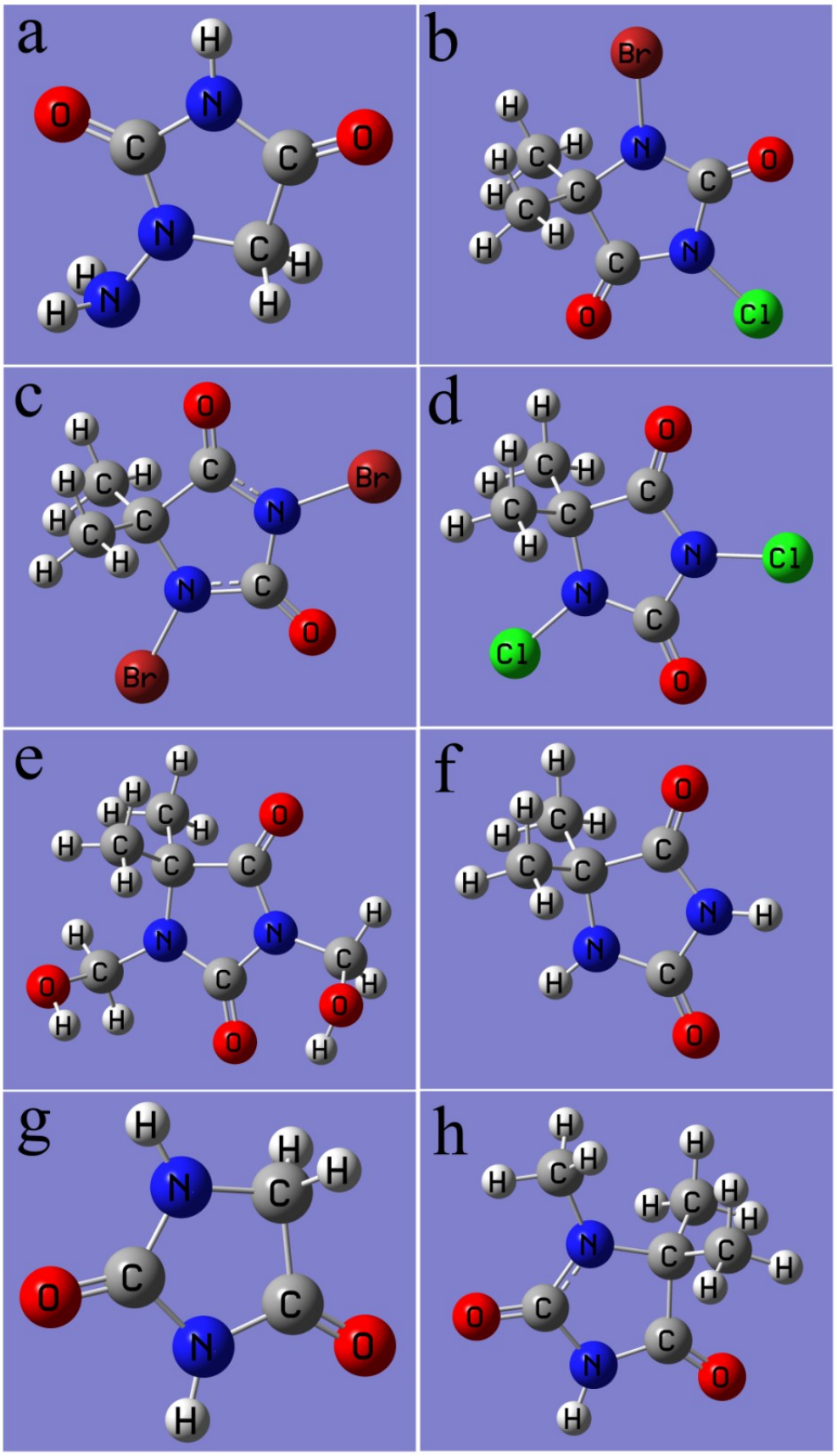

Fig. S4 Molecular structures of (a) AHD, (b) BCDMH, (c) DBDMH, (d) DCDMH, (e) DMDMH, (f) DMH, (g) Hydantoin, (h) TMH.

As shown in Fig. S4, all these studied organics have the same nitrogen containing five-membered ring with the same C=O bond and different substituents, which might generate diversiform influences on the electronic properties and frontier molecular orbital information of all these studied organics. It indicated that these organic molecules showed different ability to form gold-complex coordinated bonds and adsorb on the metal surfaces due to their probable different electronic properties and frontier molecular orbital information. Quantum chemical calculations were conducted to reveal the electronic properties and frontier molecular orbital information of all these studied organics to verify the conjecture.

Fig. S5 exhibits the distribution of the HOMO and electron cloud densities of the studied hydantoin and its usual derivatives. The distribution of LUMO is displayed in Fig. S6. The presence of nitrogen and oxygen atoms showed significant contributions to the HOMO as displayed in Fig. S5. This was due to the electron donating properties of the nitrogen and oxygen atoms, resulting in the ability to form gold-complex coordinated bonds. With the replacement of hydrogen atoms by chlorine atoms, bromine atoms or methylol, BCDMH, DBDMH, DCDMH, and DMDMH manifested more complicated localization of HOMO than DMH, as displayed in Fig. S5 (b) ~ (d), (e) and (f). Molecules (b) ~ (d) in Fig. S6 show a similar localization of the LUMO and high electron cloud densities, indicating similar electronic properties and strong electron accepting abilities. On the other hand, molecules (a) possessed the similar electronic properties and electron accepting abilities with molecules (e) ~ (h).

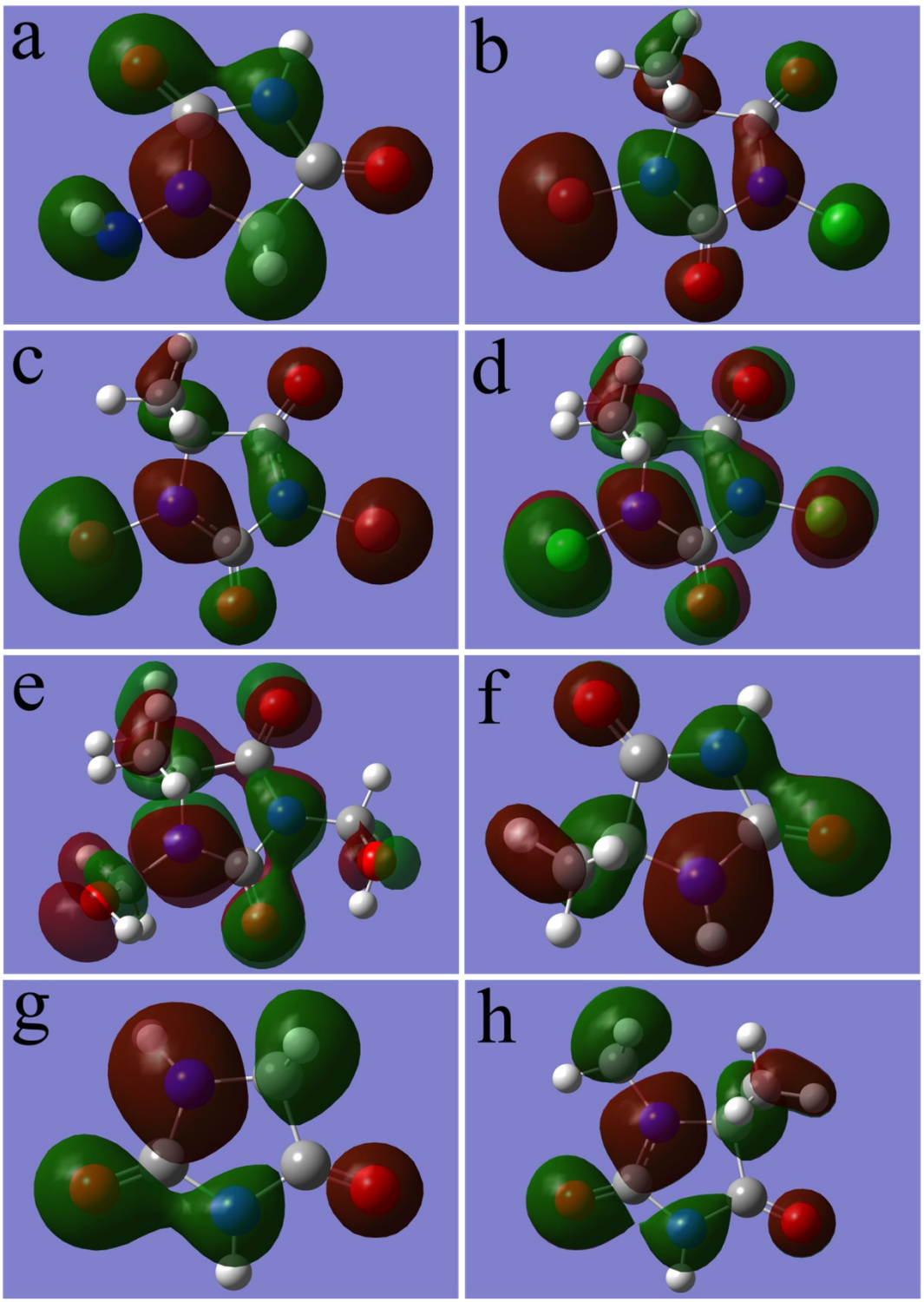

Fig. S5 Localization of the highest occupied molecular orbital (HOMO) of (a) AHD, (b) BCDMH, (c) DBDMH, (d) DCDMH, (e) DMDMH, (f) DMH, (g) Hydantoin, (h) TMH.

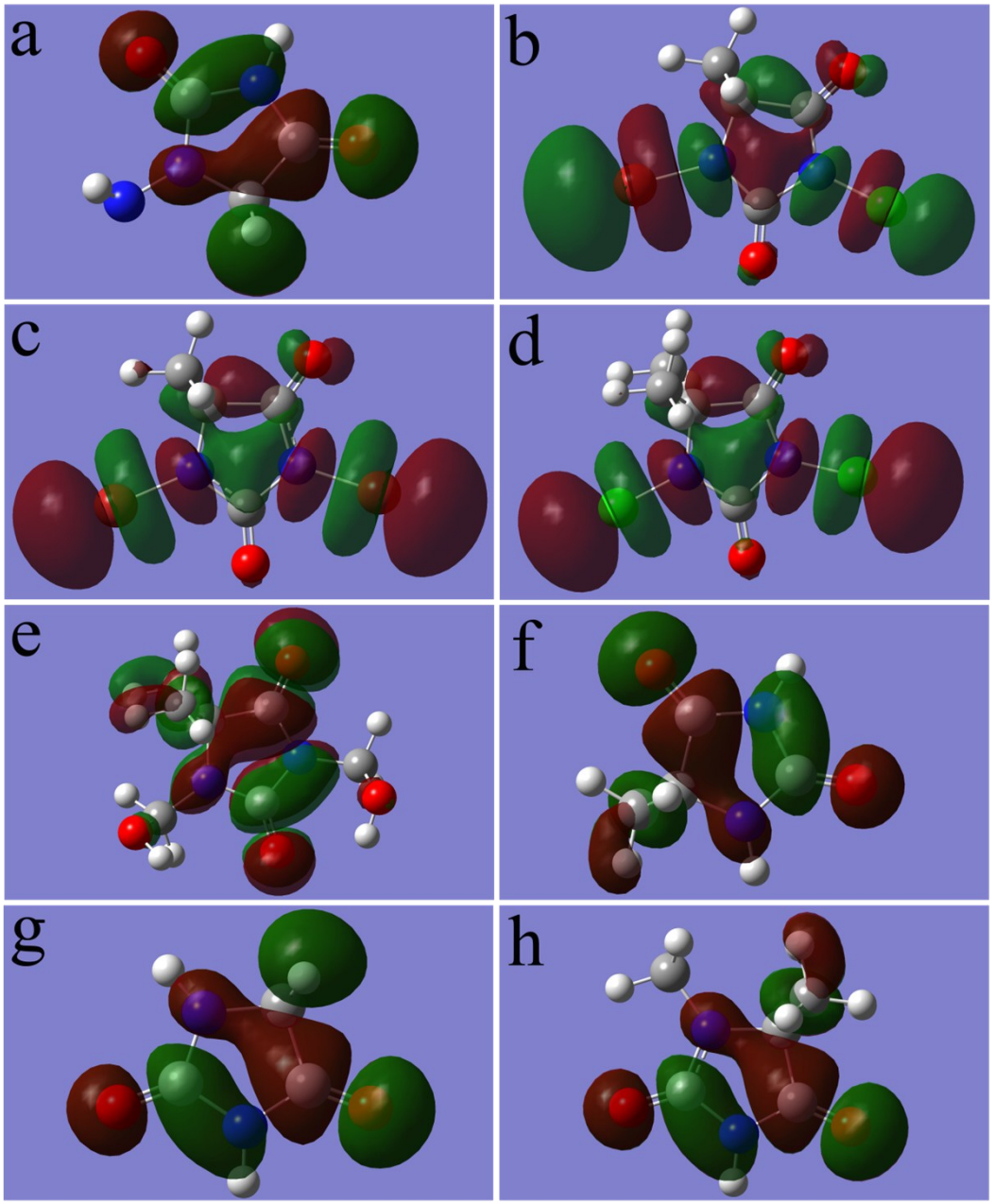

Fig. S6 Localization of the lowest unoccupied molecular orbital (LUMO) of (a) AHD, (b) BCDMH, (c) DBDMH, (d) DCDMH, (e) DMDMH, (f) DMH, (g) Hydantoin, (h) TMH.

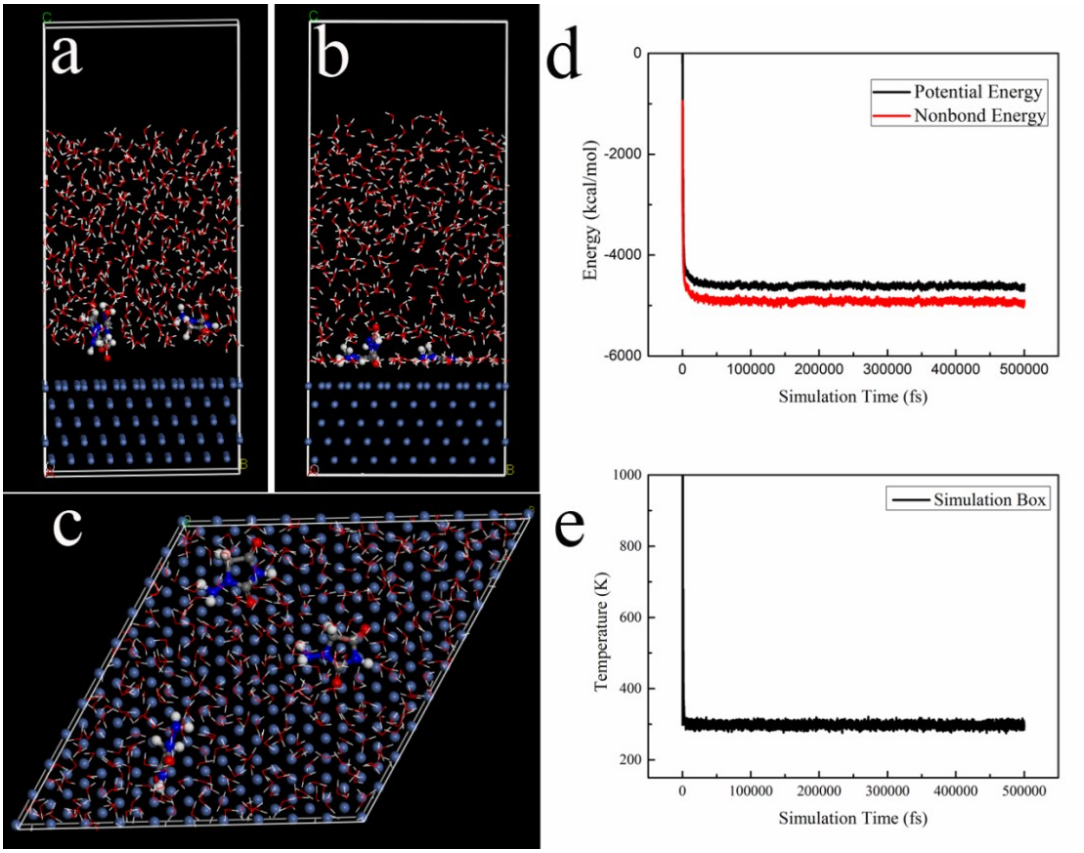

Fig. S7 Adsorption behaviors of AHD on the Ni surface, (a) Initial configuration of the simulation box (AHD visualized by balls and sticks, water molecule visualized by lines). (b) Final equilibrium configuration of the MD simulation box. (c) Top view of the final equilibrium configuration of the simulation box. (d) Energy fluctuation curves of the MD simulation. (e) Temperature fluctuation curve of the MD simulation.

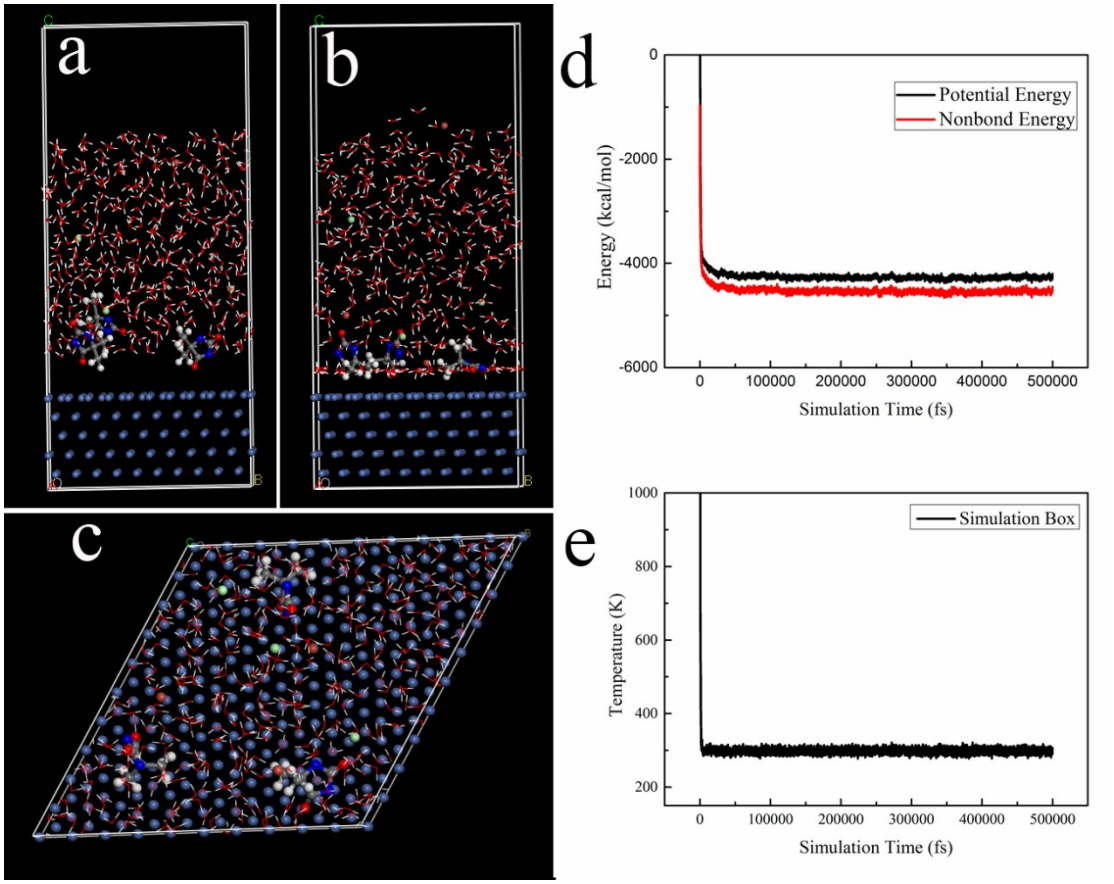

Fig. S8 Adsorption behaviors of BCDMH on the Ni surface, (a) Initial configuration of the simulation box (BCDMH visualized by balls and sticks, water molecule visualized by lines). (b) Final equilibrium configuration of the MD simulation box. (c) Top view of the final equilibrium configuration of the simulation box. (d) Energy fluctuation curves of the MD simulation. (e) Temperature fluctuation curve of the MD simulation.

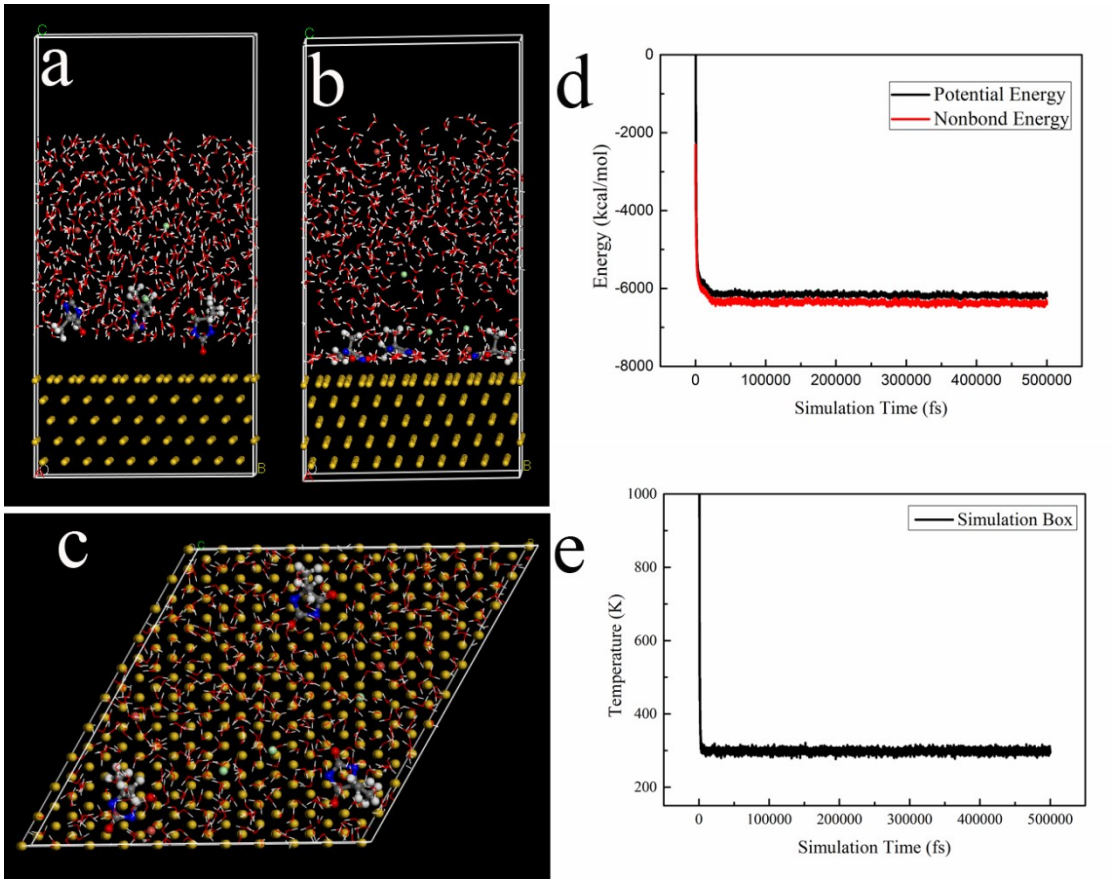

Fig. S9 Adsorption behaviors of BCDMH on the Au surface, (a) Initial configuration of the simulation box (BCDMH visualized by balls and sticks, water molecule visualized by lines). (b) Final equilibrium configuration of the MD simulation box. (c) Top view of the final equilibrium configuration of the simulation box. (d) Energy fluctuation curves of the MD simulation. (e) Temperature fluctuation curve of the MD simulation.

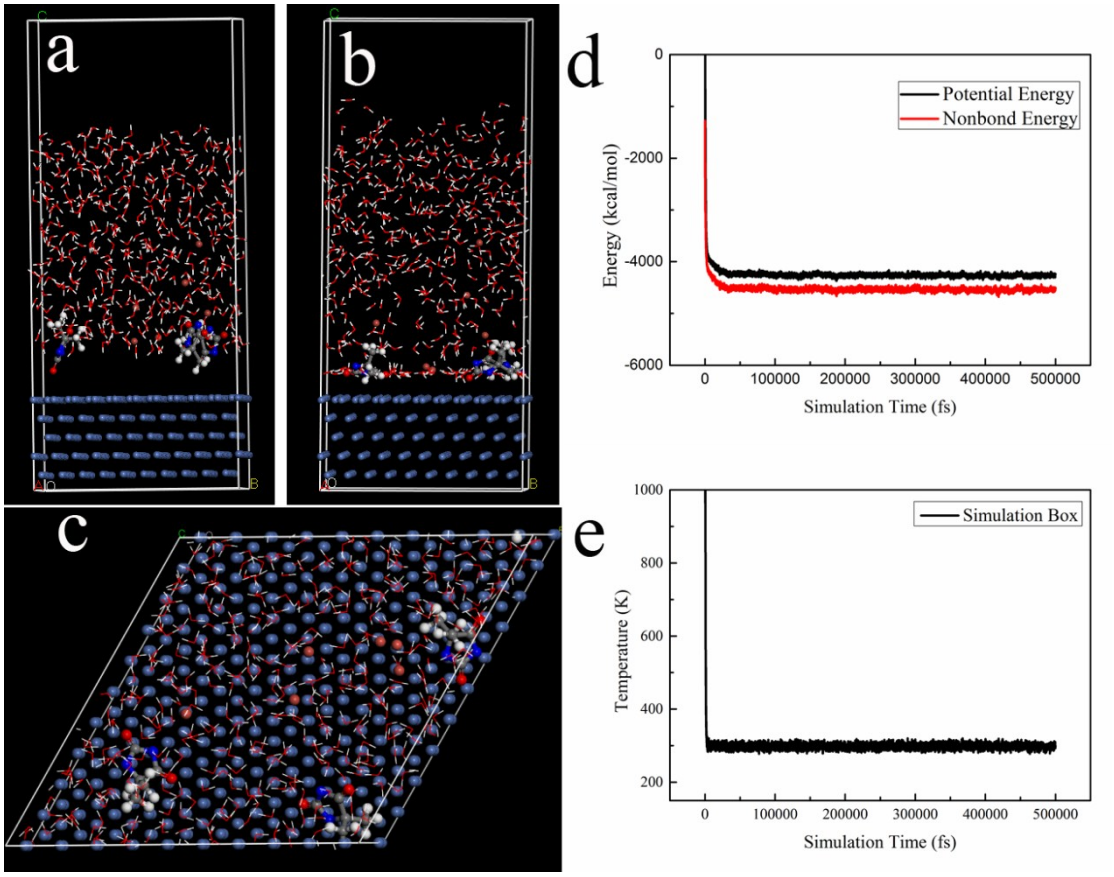

Fig. S10 Adsorption behaviors of DBDMH on the Ni surface, (a) Initial configuration of the simulation box (DBDMH visualized by balls and sticks, water molecule visualized by lines). (b) Final equilibrium configuration of the MD simulation box. (c) Top view of the final equilibrium configuration of the simulation box. (d) Energy fluctuation curves of the MD simulation. (e) Temperature fluctuation curve of the MD simulation.

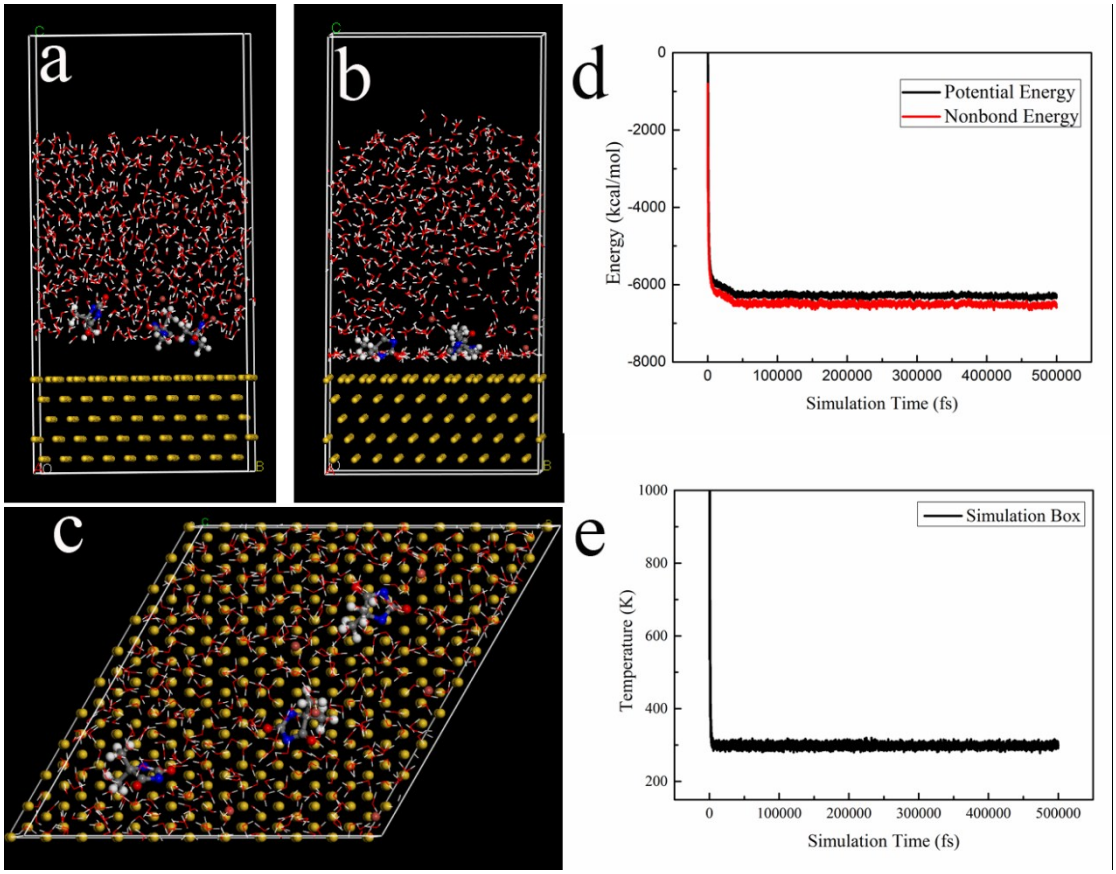

Fig. S11 Adsorption behaviors of DBDMH on the Au surface, (a) Initial configuration of the simulation box (DBDMH visualized by balls and sticks, water molecule visualized by lines). (b) Final equilibrium configuration of the MD simulation box. (c) Top view of the final equilibrium configuration of the simulation box. (d) Energy fluctuation curves of the MD simulation. (e) Temperature fluctuation curve of the MD simulation.

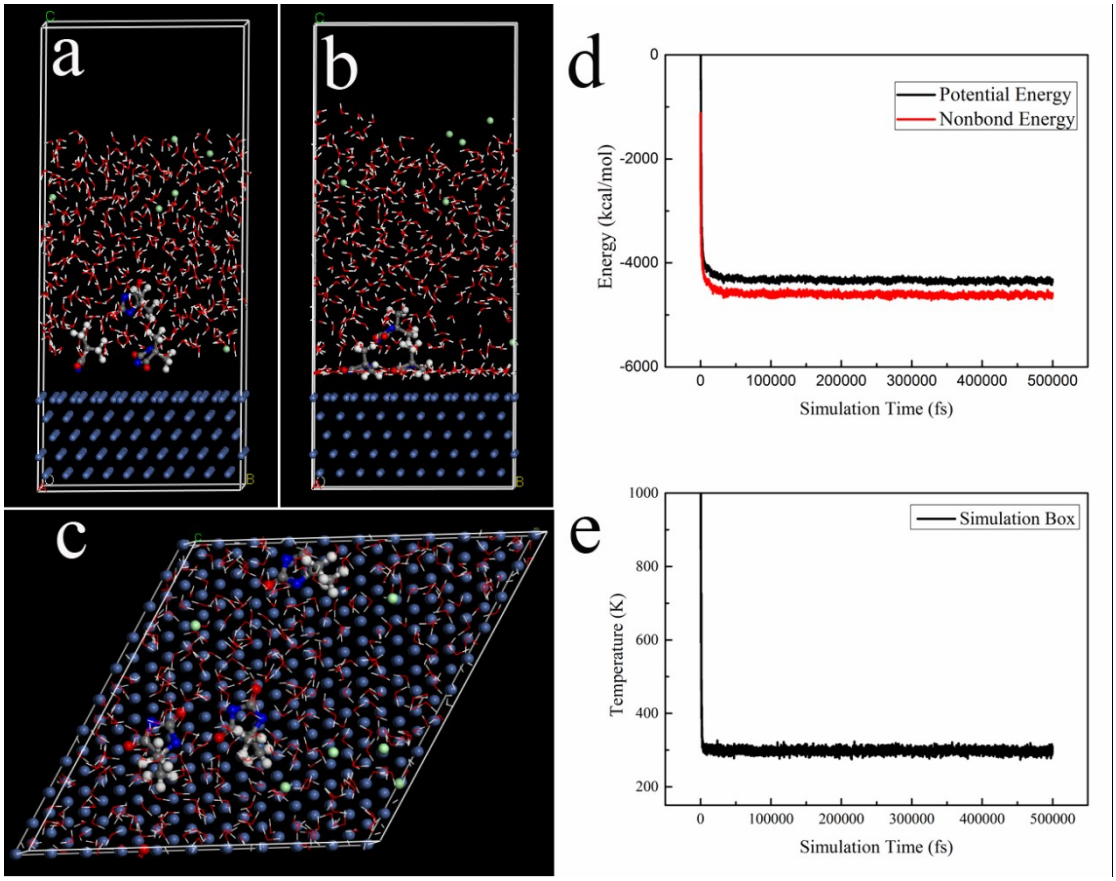

Fig. S12 Adsorption behaviors of DCDMH on the Ni surface, (a) Initial configuration of the simulation box (DCDMH visualized by balls and sticks, water molecule visualized by lines). (b) Final equilibrium configuration of the MD simulation box. (c) Top view of the final equilibrium configuration of the simulation box. (d) Energy fluctuation curves of the MD simulation. (e) Temperature fluctuation curve of the MD simulation.

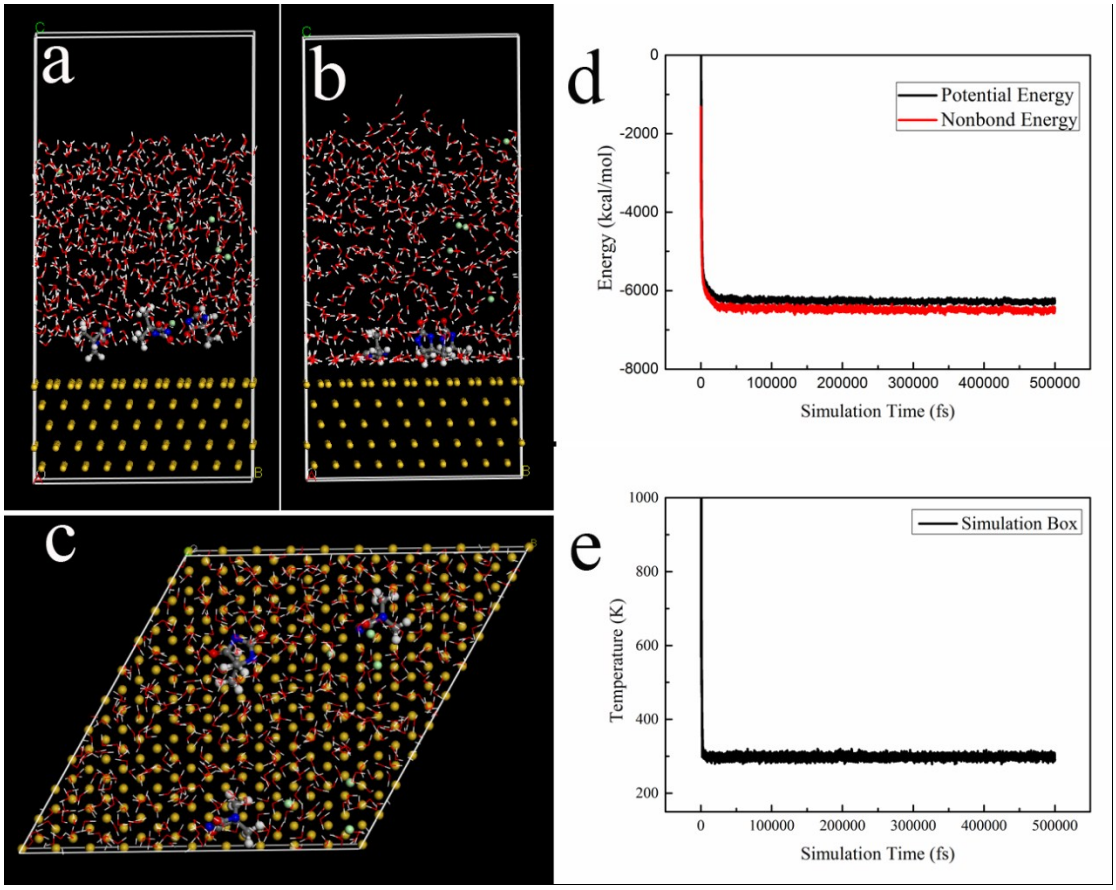

Fig. S13 Adsorption behaviors of DCDMH on the Au surface, (a) Initial configuration of the simulation box (DCDMH visualized by balls and sticks, water molecule visualized by lines). (b) Final equilibrium configuration of the MD simulation box. (c) Top view of the final equilibrium configuration of the simulation box. (d) Energy fluctuation curves of the MD simulation. (e) Temperature fluctuation curve of the MD simulation.

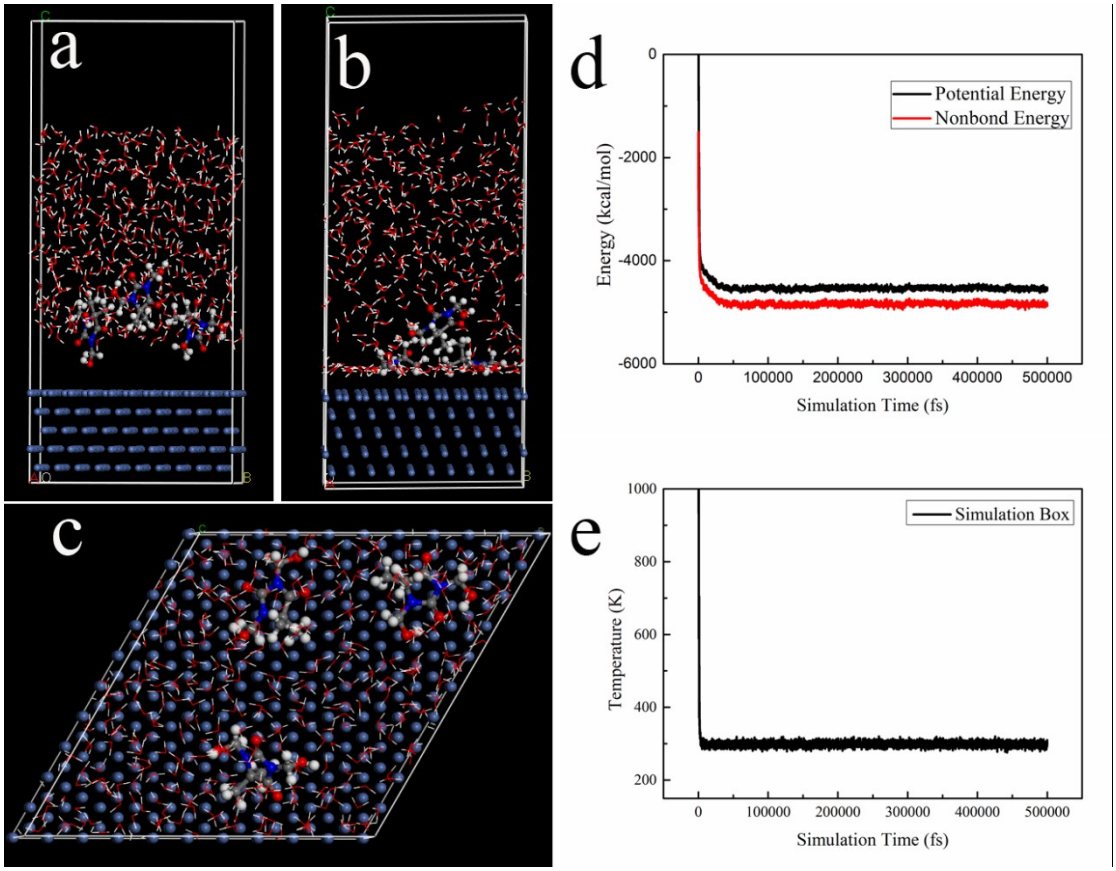

Fig. S14 Adsorption behaviors of DMDMH on the Ni surface, (a) Initial configuration of the simulation box (DMDMH visualized by balls and sticks, water molecule visualized by lines). (b) Final equilibrium configuration of the MD simulation box. (c) Top view of the final equilibrium configuration of the simulation box. (d) Energy fluctuation curves of the MD simulation. (e) Temperature fluctuation curve of the MD simulation.

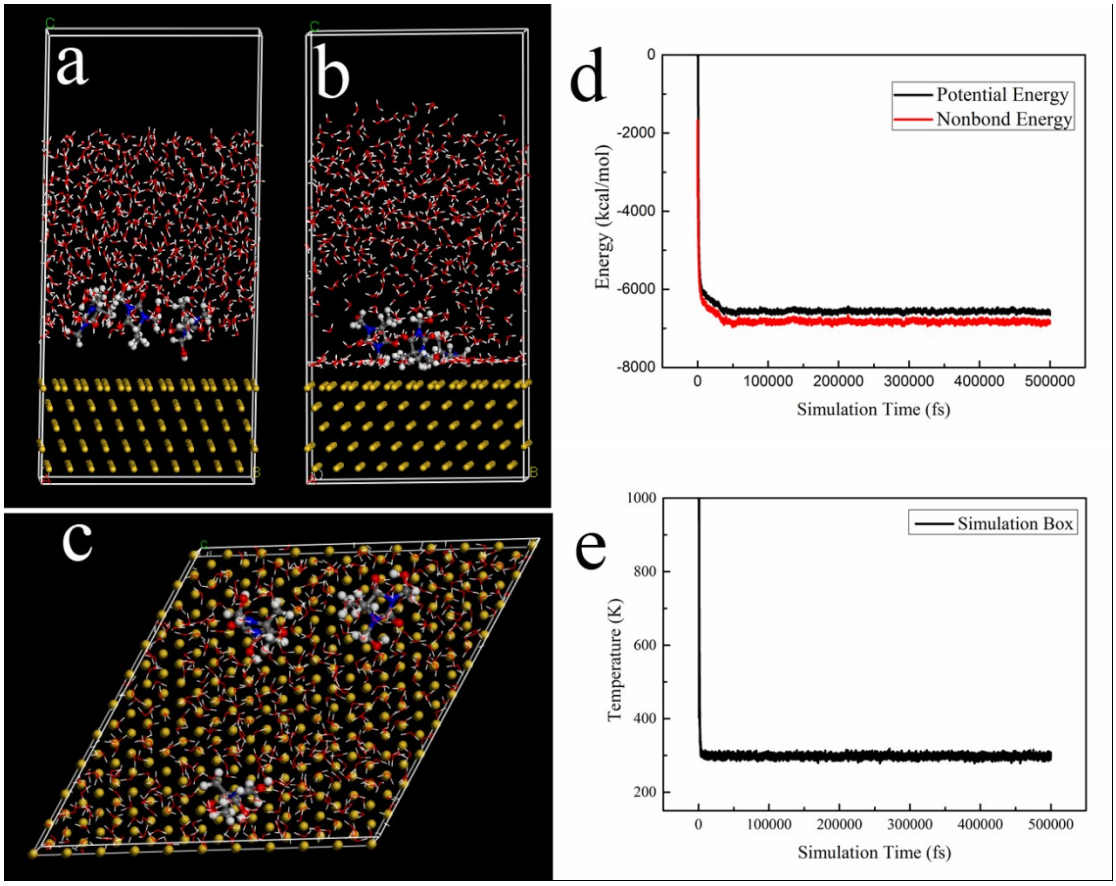

Fig. S15 Adsorption behaviors of DMDMH on the Au surface, (a) Initial configuration of the simulation box (DMDMH visualized by balls and sticks, water molecule visualized by lines). (b) Final equilibrium configuration of the MD simulation box. (c) Top view of the final equilibrium configuration of the simulation box. (d) Energy fluctuation curves of the MD simulation. (e) Temperature fluctuation curve of the MD simulation.

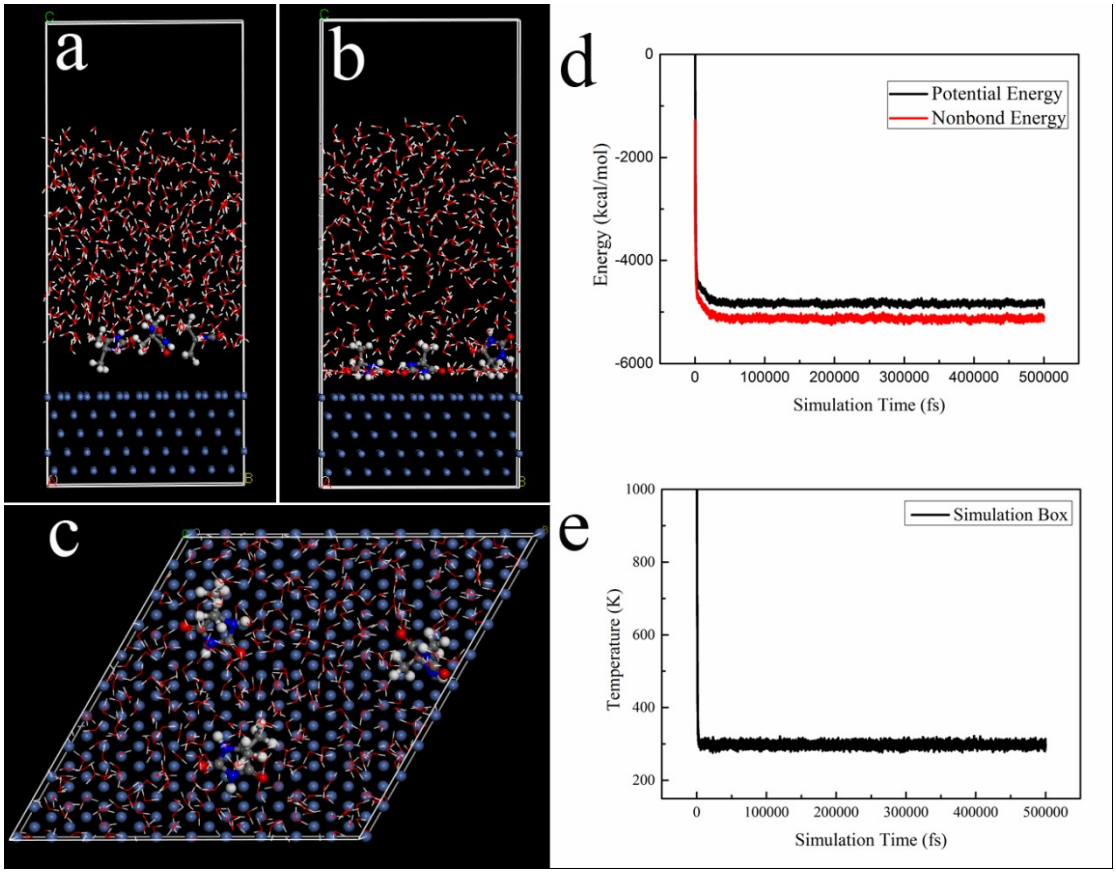

Fig. S16 Adsorption behaviors of DMH on the Ni surface, (a) Initial configuration of the simulation box (DMH visualized by balls and sticks, water molecule visualized by lines). (b) Final equilibrium configuration of the MD simulation box. (c) Top view of the final equilibrium configuration of the simulation box. (d) Energy fluctuation curves of the MD simulation. (e) Temperature fluctuation curve of the MD simulation.

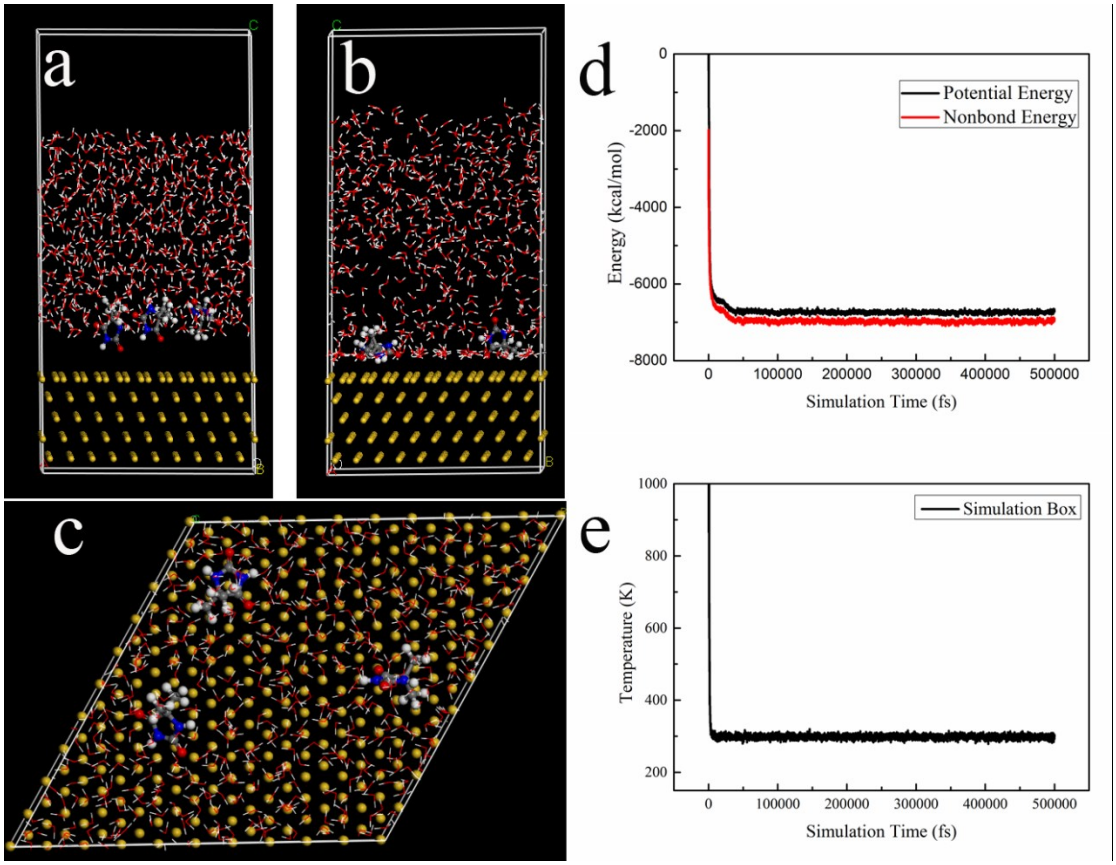

Fig. S17 Adsorption behaviors of DMH on the Au surface, (a) Initial configuration of the simulation box (DMH visualized by balls and sticks, water molecule visualized by lines). (b) Final equilibrium configuration of the MD simulation box. (c) Top view of the final equilibrium configuration of the simulation box. (d) Energy fluctuation curves of the MD simulation. (e) Temperature fluctuation curve of the MD simulation.

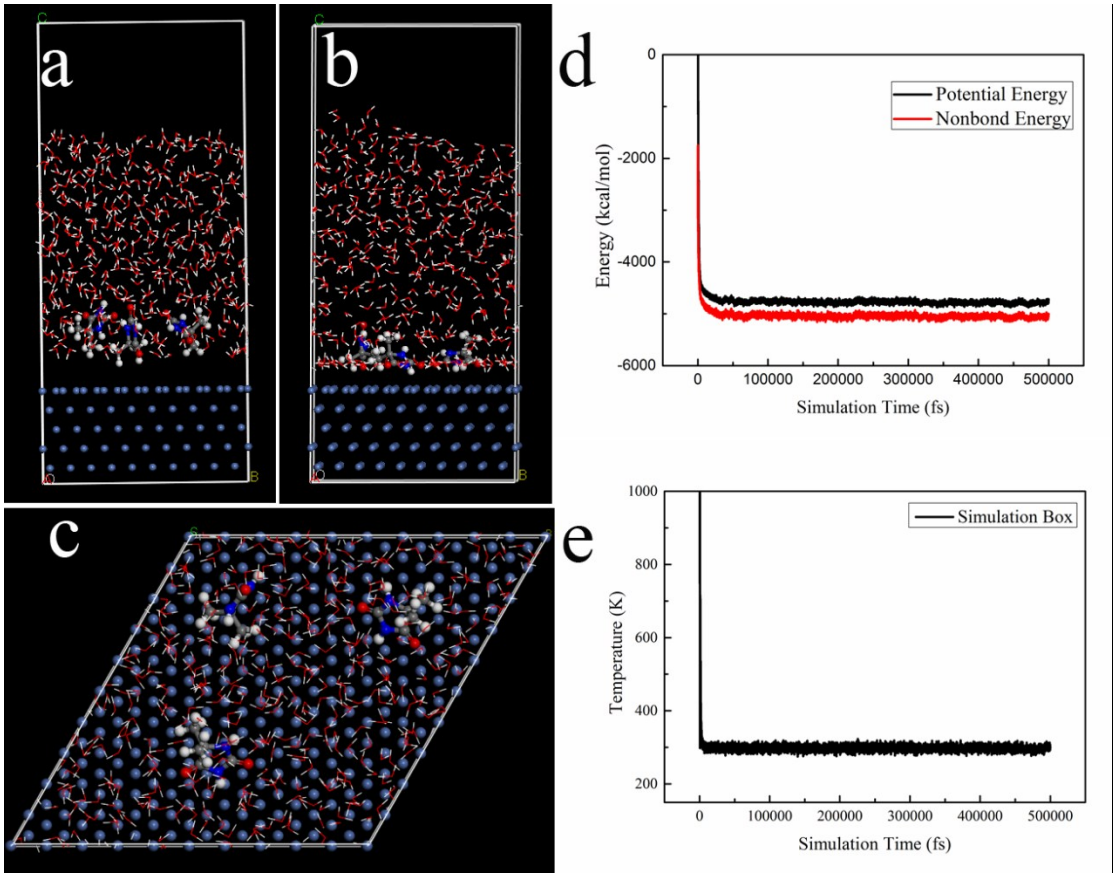

Fig. S18 Adsorption behaviors of Hydantoin on the Ni surface, (a) Initial configuration of the simulation box (Hydantoin visualized by balls and sticks, water molecule visualized by lines). (b) Final equilibrium configuration of the MD simulation box. (c) Top view of the final equilibrium configuration of the simulation box. (d) Energy fluctuation curves of the MD simulation. (e) Temperature fluctuation curve of the MD simulation.

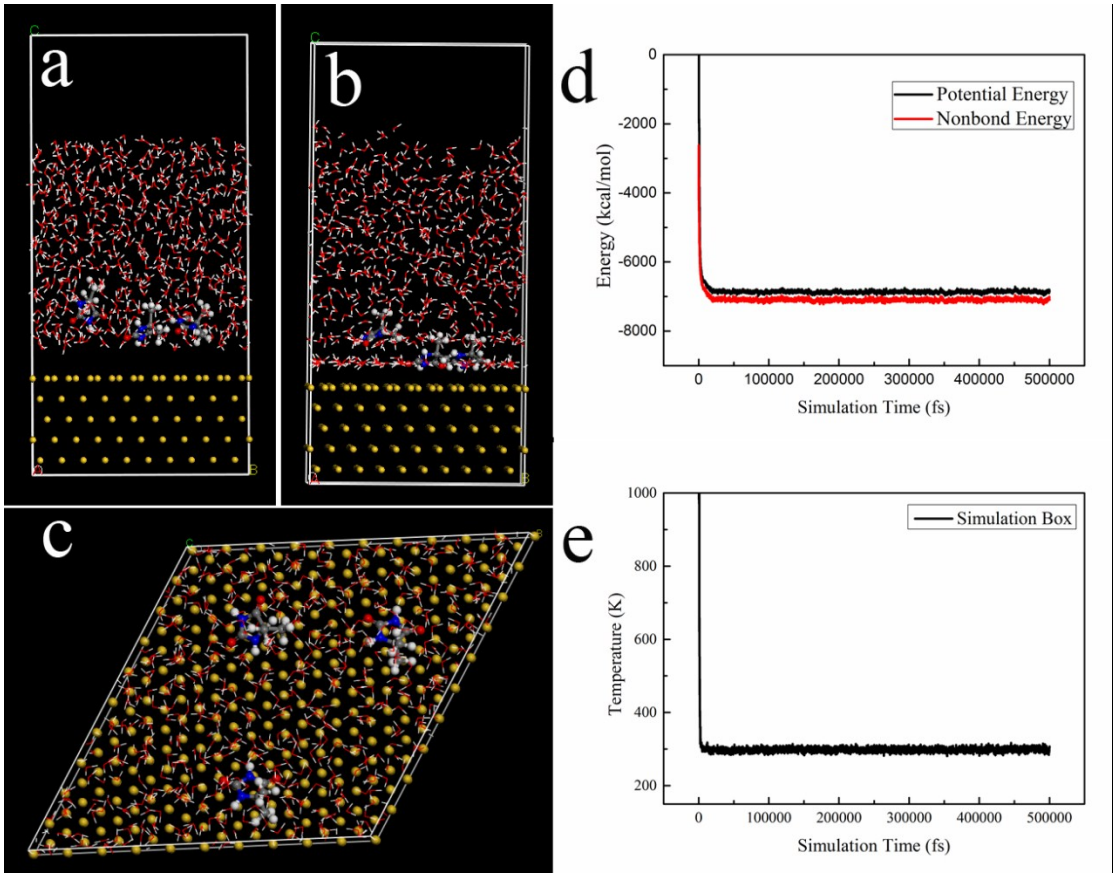

Fig. S19 Adsorption behaviors of Hydantoin on the Au surface, (a) Initial configuration of the simulation box (Hydantoin visualized by balls and sticks, water molecule visualized by lines). (b) Final equilibrium configuration of the MD simulation box. (c) Top view of the final equilibrium configuration of the simulation box. (d) Energy fluctuation curves of the MD simulation. (e) Temperature fluctuation curve of the MD simulation.

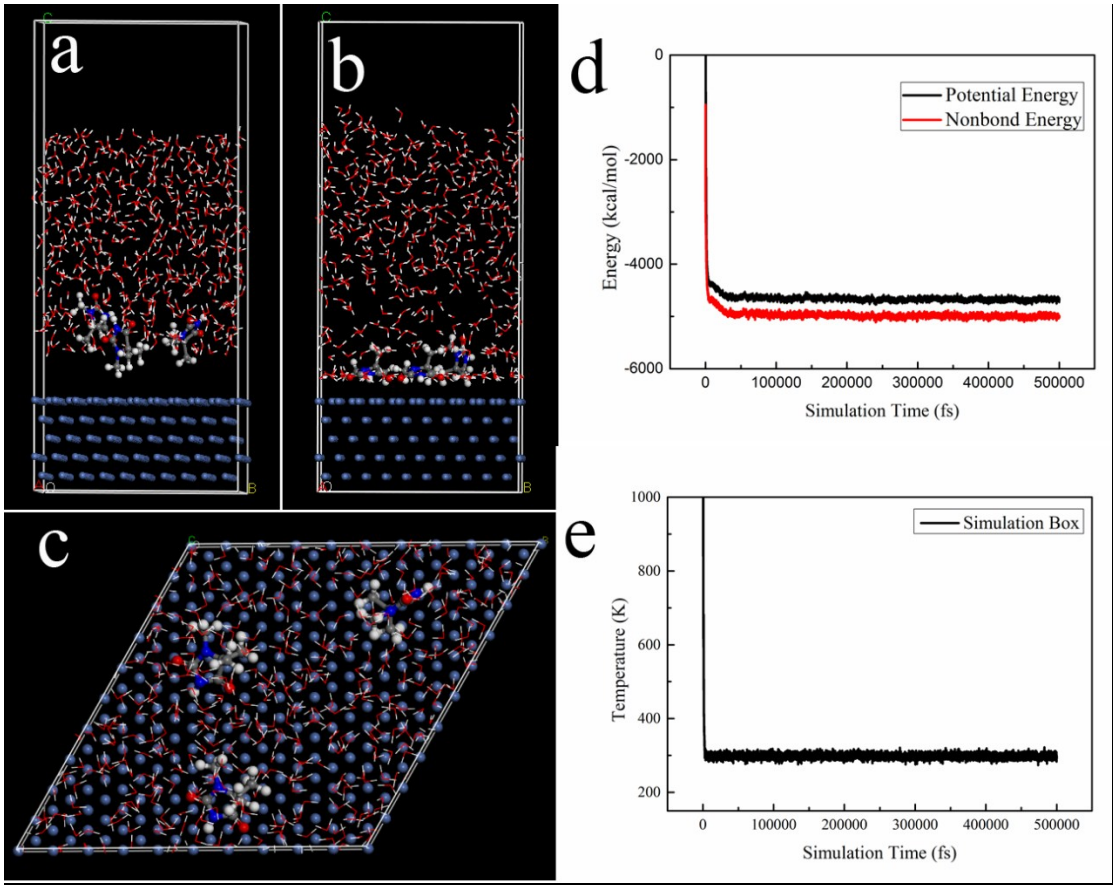

Fig. S20 Adsorption behaviors of TMH on the Ni surface, (a) Initial configuration of the simulation box (TMH visualized by balls and sticks, water molecule visualized by lines). (b) Final equilibrium configuration of the MD simulation box. (c) Top view of the final equilibrium configuration of the simulation box. (d) Energy fluctuation curves of the MD simulation. (e) Temperature fluctuation curve of the MD simulation.

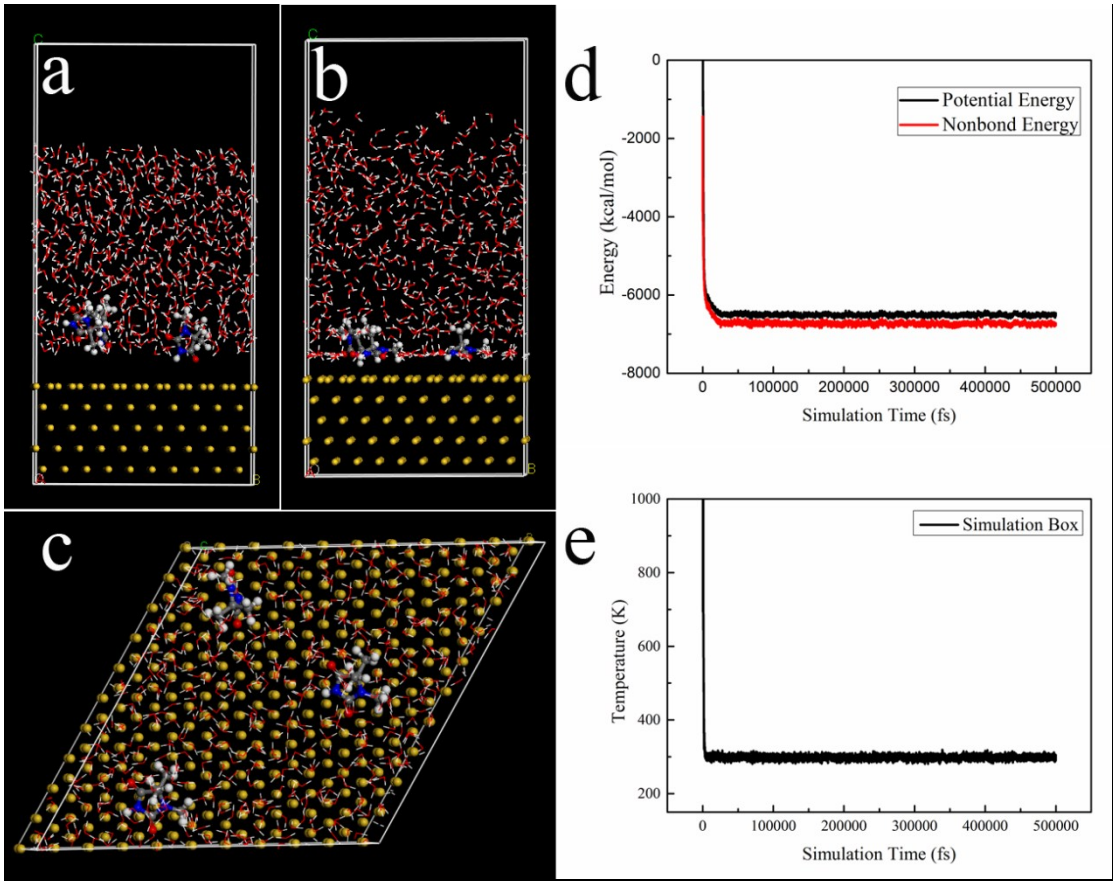

Fig. S21 Adsorption behaviors of TMH on the Au surface, (a) Initial configuration of the simulation box (TMH visualized by balls and sticks, water molecule visualized by lines). (b) Final equilibrium configuration of the MD simulation box. (c) Top view of the final equilibrium configuration of the simulation box. (d) Energy fluctuation curves of the MD simulation. (e) Temperature fluctuation curve of the MD simulation.